Rotation capacity of self-compacting steel fibre reinforced concrete beams

Petra Schumacher, Joost C. Walraven, Joop A. den Uijl
Faculty of Civil Engineering and Geosciences, Delft University of Technology,
The Netherlands

Agnieszka Bigaj-van Vliet
TNO Built Environment and Geosciences, The Netherlands

Steel fibres are known to enhance the toughness of concrete in compression and in tension. Steel fibres also improve the bond properties between concrete matrix and reinforcing steel bars. In order to investigate the effect of steel fibres on the rotation capacity of reinforced concrete members, four simply supported beams were loaded in three-point bending up to failure (steel bar rupture or concrete crushing). Test variables were fibre content and axial normal force. Remarkably, the specimens with conventional reinforcement had a larger rotation capacity than those with conventional reinforcement and fibres. This decrease in deformation capacity is explained by localization of the deformations in one large crack in case of the reinforced concrete (RC) specimens with steel fibres, compared to several large cracks in case of the RC specimens. A model to calculate the rotation capacity of self-compacting steel fibre reinforced concrete (SCSFRC) members is presented and validated against the beam test results.

Key words: rotation capacity, self-compacting steel fibre reinforced concrete, strain localization

1 Introduction

According to many standards, e.g. Eurocode 2 (1992), the design of reinforced concrete (RC) structures in the Ultimate Limit State (ULS) is possible using nonlinear approaches, linear analysis with or without redistribution or the theory of plasticity. When using these approaches it has to be guaranteed that the deformation capacity provided by the structure exceeds the demand. In some cases, existing practice allows the use of some of those methods without direct verification of sufficient ductility, based on the assumption that there is sufficient ductility to balance the lack of compatibility within the limits of e.g. the

allowable degree of redistribution. In other cases, it must be verified that for the assumed mechanism the plastic rotation capacity is sufficiently large. In both cases it is essential to make sure that either the limits assigned to the specific design methods are sufficiently conservative or that the verification procedure is reliable and sound. There are various models to calculate the available rotation capacity of beams and slabs made of conventional concrete (CEB, 1998). For practical purposes, some standards (like MC90) also give simplified relationships for the available rotation capacity versus the cross sectional characteristics (e.g. x/d) for selected types of materials. Both with respect to the calculation models and more simplified relationships it is important to be sure that they are valid for the range of materials used in the specific design. Considering the development of new types of concrete, such as fibre reinforced concrete, question marks can be placed with regard to the applicability of the verification rules for rotation capacity.

The addition of fibres to concrete leads to an increase of ductility both in compression and in tension. This suggests that it might as well improve the rotation capacity of plastic hinges in concrete structures, which opens interesting possibilities for the design of concrete structures. The research project presented here aims at explaining if, and to what extent, the addition of fibres alters the rotation capacity of plastic hinges in concrete. In order to give well-founded answers, at first the influence of steel fibres was investigated and modelled with respect to the properties of concrete in compression, the properties of concrete in tension and the bond of deformed reinforcing bars embedded in self-compacting steel fibre reinforced concrete (SCSFRC). Then, the knowledge gained from this investigation was applied in developing a model for the rotation capacity of SCSFRC members. In the experiments, normal and high strength self-compacting concretes with up to 120 kg/m³ steel fibres with hooked ends, as developed by Grünewald (2004), were used.

2 Mechanical properties of SCSFRC

2.1 Influence of Steel Fibres on the Tensile Behaviour of Concrete

When investigating the influence of fibres on the concrete behaviour in tension, two major aspects should be paid attention to: the tensile strength and the post-peak behaviour. The experimental investigation confirmed that the uniaxial tensile strength is not influenced by the amount of hooked-end steel fibres used in the investigation. However, the post-peak behaviour of the concrete is improved by the addition of the fibres. This improvement depends on the:

- effective amount of fibres,
- fibre geometry (aspect ratio, fibre length),
- fibre orientation,
- fibre strength (fibre pull-out or fibre rupture),
- bond properties of fibres in concrete (matrix quality, fibre shape).

In this study, the model of Kützing (2000), which describes the softening of steel fibre reinforced concrete (SFRC), was modified and used for the calculation of the bond behaviour and rotation capacity of SCSFRC (Schumacher, 2006). The model of Kützing (2000) takes into account the slope of the first branch observed in uniaxial tension tests, the fibre content (with no fibres as a lower bound), the fibre orientation, the bond properties of the fibres and the shape and maximum size of the aggregates. The model was modified with regard to the determination of the uniaxial tensile strength (depending on the splitting tensile strength and not necessarily on the compressive strength), effect of fibre orientation, and complexity (bilinear instead of trilinear relation). The stress (σ_{ct}) versus crack width (w) relation is defined as shown in Fig. 1 by the uniaxial tensile strength f_{ct}, the critical crack width w_0 and the Fictitious Crack Model (FCM) constants α_{FCM} and β_{FCM}.

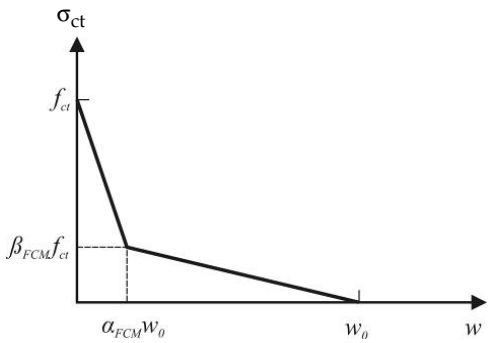

Figure 1: Definition of the parameters in the stress-crack width relation

2.2 *Influence of steel fibres on the compressive behaviour of concrete*

Failure of concrete in compression is related to failure of concrete in tension. When concrete is externally loaded in uniaxial compression, internal tensile stresses act perpendicular to the direction of the compressive load. Therefore, the behaviour of concrete in compression is influenced by similar parameters as the behaviour of concrete in tension. In the scope of this research project, normal and high strength concrete prisms

with different amounts and geometries of steel fibres were tested concentrically and eccentrically. The compressive strength was not significantly affected by the addition of fibres, but the post-peak capacity of the concrete was increased by the addition of fibres. Fig. 2 shows the experimental results of concentric compressive tests on normal strength concrete with different fibre factors $V_f\, l_f / d_f$, whereas V_f denotes the fibre content in vol.-%, l_f the fibre length and d_f the fibre diameter. In this research project, the Compressive Damage Zone (CDZ) Model developed by Markeset (1993) for plain concrete was extended to different amounts of steel fibres with different aspect ratios. The ratio between energy consumed due to opening of the longitudinal cracks in the post-peak region to that consumed in the pre-peak region is denoted as the factor k in the CDZ model. The value of k was 3 in the original CDZ model. For self-compacting concrete (SCC), it was proposed to be 3.5 (Schumacher, 2006). The increase of the energy consumed in the post-peak region due to fibre addition is accounted for in an additive term, see equation (1) for concentric tests.

$$k = 3.5 + 10 V_f\, l_f / d_f \tag{1}$$

Fig. 3 shows the stress-strain behaviour as modelled with the extended CDZ model for the same mixtures as referred to in Fig. 2. The increase of post-peak capacity with increasing fibre factor can be clearly seen in both figures.

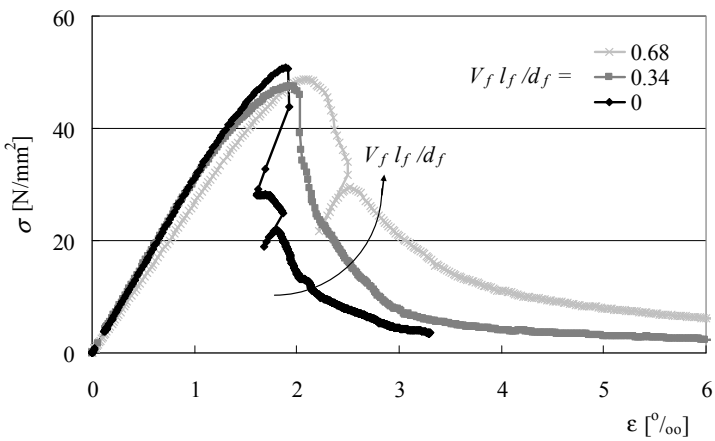

Figure 2: Influence of fibre addition on compressive behaviour for different $V_f\, l_f / d_f$ - experimental results

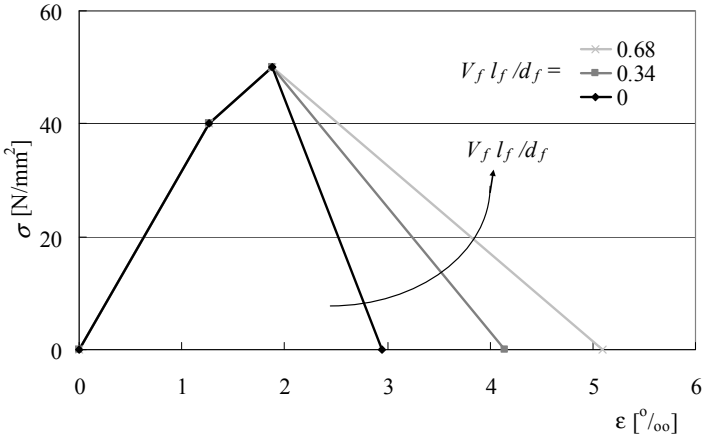

Figure 3: Influence of fibre addition on compressive behaviour for different $V_f\, l_f / d_f$ - model

3 Influence of steel fibres on the bond behaviour of reinforcing bars

3.1 General remarks

The contribution of steel fibres and reinforcing bars to the transfer of forces substantially differs. The contribution of steel fibres generally decreases with increasing crack width, whereas the contribution of reinforcing bars increases due to the hardening of the reinforcing steel as the cracks open further. A combination of steel fibres and tensile reinforcing bars can bring together the advantages of both: the reinforcing bars carry the forces in the tension chord, while the steel fibres provide a confinement of the concrete cover, prevent spalling and carry multiaxial loads (shear, partial area loading).

Since steel fibres influence the load carrying and deformation behaviour of reinforced concrete (RC) members, the validity of design rules that have been developed for RC members has to be verified. Unfortunately, many experiments on SFRC in the past only covered the range relevant for the Serviceability Limit State (SLS). In those cases, essential information for the evaluation of the structural behaviour in the range of plastic deformations is missing and the redistribution capacity of a structure cannot be evaluated. Some more recent investigations did cover the range of plastic deformations, e.g. Pfyl & Marti (2001), Eligehausen et al. (2003), Fehling & Leutbecher (2005). The investigation reported in Schumacher (2006) included a complementary study on the bond behaviour in tensile members and the load-deformation behaviour in bending members made of SCSFRC.

3.2 *Effect of steel fibres on the bond stress-slip relation*

The main factors influencing the bond behaviour of a reinforcing bar in a concrete matrix are concrete tensile properties (strength and ductility), bar surface geometry, bar diameter, concrete cover thickness, position of the bar during casting, state of stress in the bar, state of stress in the surrounding concrete and boundary conditions. Steel fibres influence the properties of the concrete and thereby the confinement capacity of the concrete surrounding a reinforcing bar. Steel fibres also influence the stress level in the reinforcing bars and the surrounding concrete by transferring stresses across the cracks.

Two types of bond failure can be distinguished: splitting failure and pull-out failure. The failure mode depends on the confinement provided by the surrounding concrete, confining reinforcement and external pressure. For the practical application of the present research project, i.e. tunnelling, pull-out failure is expected to be relevant because of the small bar diameters and the relatively large concrete covers used. In case of pull-out failure, the concrete keys between the ribs are sheared off and a sliding plane around the bar is created. After shearing off of the concrete keys, the force transfer mechanism changes from rib bearing to friction along the cylindrical sliding plane. When the loading is continued, the sliding plane is smoothened due to wear and compaction of the concrete. The maximum bond stress in case of pull-out failure follows from the tensile strength of the concrete and depends on the steel stress (Den Uijl & Bigaj, 1996; Bigaj, 1999).

In the scope of this research project (Schumacher, 2006), pull-out tests were performed on ribbed bars (d_s = 10 mm) in a self-compacting normal strength concrete without steel fibres and with 60 kg/m³ fibres (geometry l_f/d_f = 80 and l_f = 30 mm). The concrete cover was varied (c = 15, 25, 35, 95 mm). Except for one specimen without steel fibres and a concrete cover of 15 mm, all specimens presented pull-out failure without visible splitting cracks. The influence of steel fibres in case of pull-out failure was small. Considering the scatter of the test results, the influence of steel fibres on the bond stress-slip relation is neglected in the modelling in case of pull-out bond failure.

3.3 *Effect of steel fibres on the stress transfer across cracks*

The post-cracking behaviour of SFRC is one of the significant differences between plain concrete and SFRC. While in plain concrete the contribution of the concrete to the stress transfer in cracks is often neglected, it needs to be considered in modelling SFRC. Steel fibres transfer stresses across the cracks. This stress is a function of the crack width.

The magnitude of the force transmitted by a fibre depends on the bond between fibre and matrix and can be limited by the fibre tensile strength (see Marković et al., 2002; Van Gysel,

2000; Pfyl, 2003). Single fibre pull-out tests on the mixtures used in the scope of this research were carried out by Marković et al. (2002).

The transmission length L_t is defined as the length required for developing the concrete tensile strength in a cross-section. The average crack distance s_{cr} is assumed to be 1.3 times the transmission length. The influence of steel fibres on the transfer length L_t is illustrated in Fig. 4. The SFRC stress in the crack is not zero but depends on the crack width w. As the bond stress-slip relation in case of pull-out failure is approximately identical for concrete with and without steel fibres, the concrete stresses are built up in a similar way in both types of concrete. Due to the different stress conditions in a crack as explained before, the tensile strength is reached after a shorter transfer length L_{tf} in SFRC compared to plain concrete (Niemann, 2002). Therefore, the crack spacing and crack widths in the SLS are smaller in SFRC than in RC. A member with steel fibres is stiffer than a similar member without steel fibres.

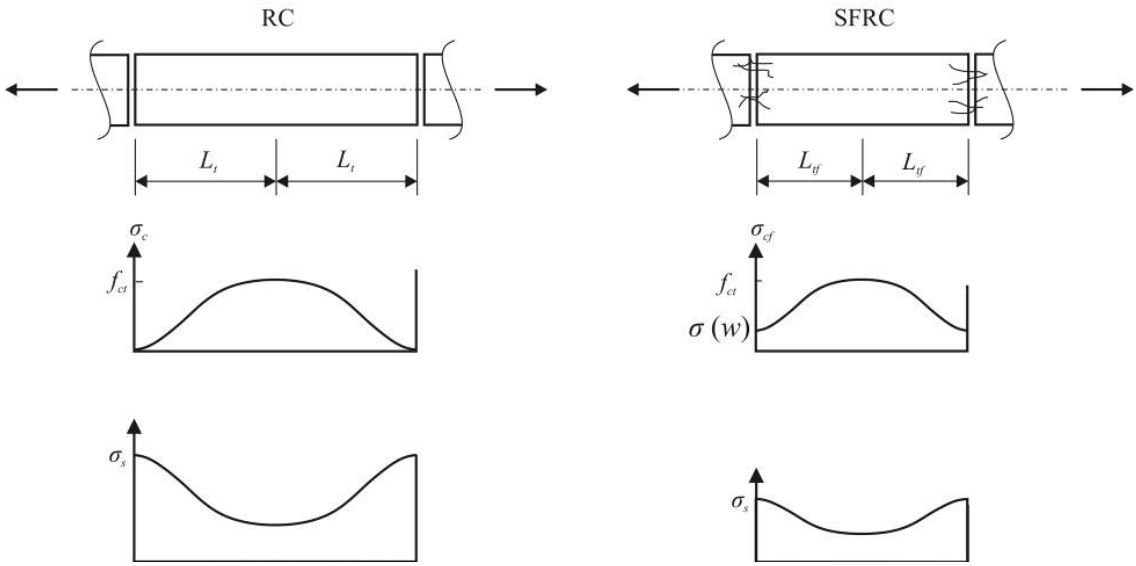

Figure 4: Stress development in RC without fibres (left) and with fibres (right): stresses in concrete (above) and in reinforcing steel (below)

4 Bond modelling

4.1 General description of the model

The analytical bond model of Den Uijl & Bigaj (1996; Bigaj, 1999) is a general bond model for ribbed bars based on confinement delivered by the concrete surrounding the reinforcing bar which is conceived as a thick-walled cylinder. The response of the thick-walled cylinder to the radial displacement of the bar-concrete interface is a radial stress at the interface. This radial displacement represents the wedging action of the ribbed bar and the radial deformation connected to the Poisson effect and is modelled by conceiving the ribbed bar as conical. The bond stress is related to the radial stress by assuming a frictional mechanism. The model takes into account the:

- bond failure mode,
- mechanism of force transfer from the ribbed bar to the surrounding concrete,
- capacity of the concrete to resist radial compressive forces, i.e. the confinement capacity,
- concrete properties (tensile strength and softening),
- state of stresses and contraction of reinforcement (especially important after yielding),
- bar diameter,
- member geometry,
- boundary effects (e.g. cone pull-out).

The model was modified to be applicable for SCSFRC with regard to the following aspects:

- the contribution of the steel fibres to the stress transfer across the cracks,
- the input of the stress-crack opening relation for SCSFRC in tension (f_{ct}, w_0, α_{FCM} and β_{FCM}),
- boundary effects (more or less prone to cone pull-out),
- an increase in the parameter τ_{b1}, which determines whether splitting or pull-out failure occurs (5% increase due to the different matrix characteristics of SCC compared to conventional concrete).

The model was verified against the results of experiments (Schumacher, 2006):

4.2 ***Transmission length***

The steel and concrete stress development along the transmission length depends on the bond between steel and concrete. The differential equation for bond is solved with a finite difference calculation. This procedure is done in the following steps. In the model, the transmission length is subdivided into 50 elements with a finite length Δx. Such an element is shown in Fig. 5.

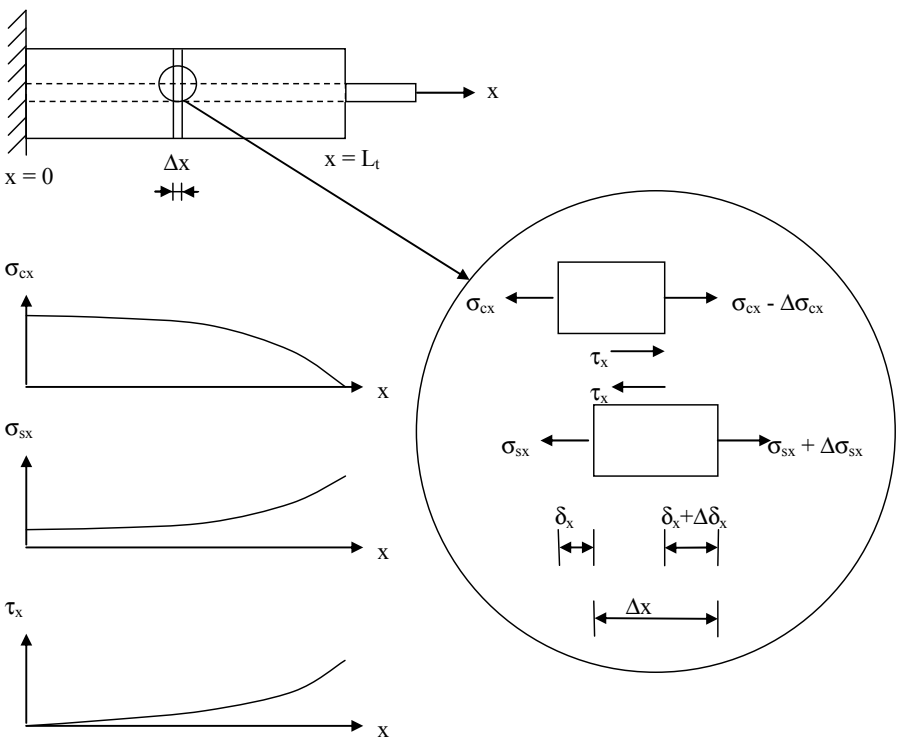

Figure 5: Equilibrium of stresses in a bar element and concrete stresses, steel stresses and bond stresses along the transmission length

The following boundary conditions apply:

- The total force along the transmission length is constant.
- The slip δ_x at the beginning of the transmission length ($x = 0$) is zero.
- The concrete stress at the beginning of the transmission length ($x = 0$) is equal to the uniaxial tensile strength.

- The concrete stress at the end of the transmission length ($x = L_t$) has a value that depends on the crack width.

The total force T in the tensile member is calculated as:

$$T = f_{ct}\, A_{c,eff}(1 + n_E\, \omega_s) \tag{2}$$

where:

T Total force in the tensile member [N]

f_{ct} Concrete tensile strength [N/mm²]

$A_{c,eff}$ Effective concrete area [mm²]

n_E Ratio of the E-moduli of steel and concrete E_s / E_c [-]

ω_s Mechanical reinforcement ratio [-]

Equilibrium of forces and compatibility of deformations has to be satisfied in each element. The steel stress at position $x = 0$ is calculated as:

$$\sigma_{s,0} = f_{ct} \frac{E_s}{E_c} \tag{3}$$

From the steel and concrete stresses, the elongations of the steel and the concrete can be calculated. The increase in slip over the element can be calculated as:

$$\Delta\delta_x = \varepsilon_{sx}\Delta x - \varepsilon_{cx}\Delta x \tag{4}$$

where:

ε_{sx} steel strain

ε_{cx} concrete strain

The bond stress τ_b is derived from the slip δ_x and the steel strain. With this bond stress, the differences in steel and concrete stresses can be calculated, using the equilibrium of forces. The increase of the steel stress can be calculated by:

$$\Delta\sigma_{sx} = \frac{\tau_b U_s \Delta x}{A_s} \tag{5}$$

where:

$\Delta\sigma_{sx}$ change in steel stress

τ_b bond stress

U_s circumference of the reinforcing bar

A_s cross-section of the reinforcing bar

As the steel stress is increased, the concrete stress is decreased:

$$\Delta\sigma_{cx} = \frac{\tau_b U_s \Delta x}{A_c} \tag{6}$$

where $\Delta\sigma_{cx}$ is the change in concrete stress.

In the iterative calculation procedure, the transmission length is found when the solution satisfies the boundary conditions. The slip at the end of the transmission length follows from the integration of the differences of steel and concrete strains. For a fully developed crack pattern, the average crack distance s_{cr} is assumed to be 1.3 times the transmission length.

4.3 Stress and strain distribution between subsequent cracks

A significant difference between SFRC and RC is that in SFRC the tensile member force is not necessarily steadily increasing with increasing elongation in the steel yielding range. On the other hand, the slip is steadily increasing and therefore it was chosen as input in the calculation of the stress and strain distribution in an element between two subsequent cracks. It is assumed that the slip at a crack is equal to half the crack width. The differential equation of bond in the calculation of the stress and strain distribution in an element between two subsequent cracks is solved with finite difference calculus. The concrete stresses in the cracks follow the stress-crack width relation. For a predefined slip,

the steel stress in the first crack is varied in a number of iterations until equilibrium of forces is found and the tensile forces at both cracks are equal.

5 Localization of deformations

It has already been observed in the past that in SFRC the plastic deformations may localize in only one crack (Pfyl & Marti, 2001; Pfyl, 2003; Eligehausen et al., 2003). On the other hand, in the usually considered serviceability range, the addition of fibres indeed leads to smaller crack widths, smaller crack spacings and a stiffer behaviour of tension elements. The response of a member with combined reinforcement depends on the stress-strain behaviour of the steel and the crack bridging force versus crack opening of the SFRC. The hardening of the reinforcing steel competes with the softening of the SFRC. The overall behaviour depends on the combination of the two. A low hardening ratio or even softening of the tensile member is caused by a large fibre content and/or pronounced softening and a low conventional reinforcement ratio and/or a low hardening ratio of the reinforcing steel. Overall softening is not desired in the design of reinforced concrete structures. To further investigate this phenomenon, a parameter study was carried out. A steel reinforcing bar (d_s = 10 mm, f_{sy} = 500 N/mm², E_s = 200000 N/mm², ε_{su} = 10%, hardening ratios (f_{su}/f_{sy}) 1.05, 1.10, 1.15, and 1.20) was concentrically embedded in a concrete cross section (80 × 80 mm, f_c = 50 N/mm², E_c = 34000 N/mm², f_{ct} = 3 N/mm², bilinear softening for fibre content 0, 60 and 120 kg/m³). Fig. 6 shows the tensile member force T versus crack width relation obtained with the modified bond model for a steel hardening ratio of 1.10. It can be seen that the members with steel fibres show a lower member hardening ratio than the member without steel fibres. Fig. 7 shows the member hardening ratios T_u/T_y, where T_u and T_y denote the tension member force at ultimate steel stress and at the onset of yielding of the reinforcing bars, respectively, obtained for different steel hardening ratios and fibre contents. The figure shows that the tensile member hardening is proportional to the steel hardening ratio and inversely proportional to the fibre content.

The fibre distribution and fibre orientation of SCSFRC can vary over the length of a member. Fig. 8 illustrates the difference in crack width for members with different steel hardening ratios and a variation of the fibre content along the member of ± 10%. As the maximum force in a tensile member is determined by the weakest cross section, the deformations in the stronger cross sections are found at that load level. It can be seen that the relative difference in crack width between the assumed weakest link with an assumed

fibre content of 10% below average compared to the crack width for the average fibre content is more pronounced for the low steel hardening ratio of 1.05 than for the larger steel hardening ratio of 1.20.

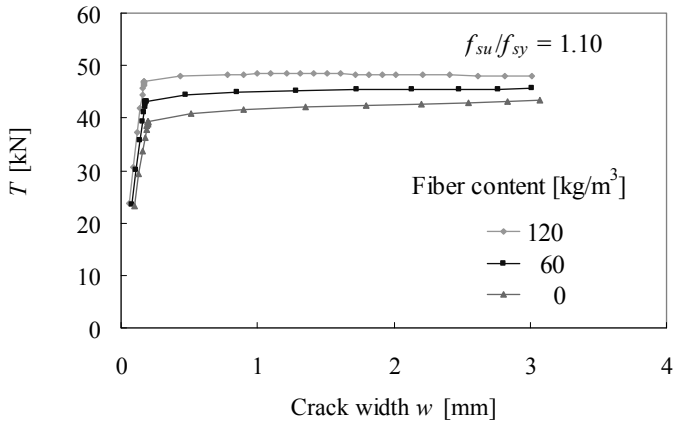

Figure 6: Relation between tensile member force and crack width for f_{su}/f_{sy} = 1.10

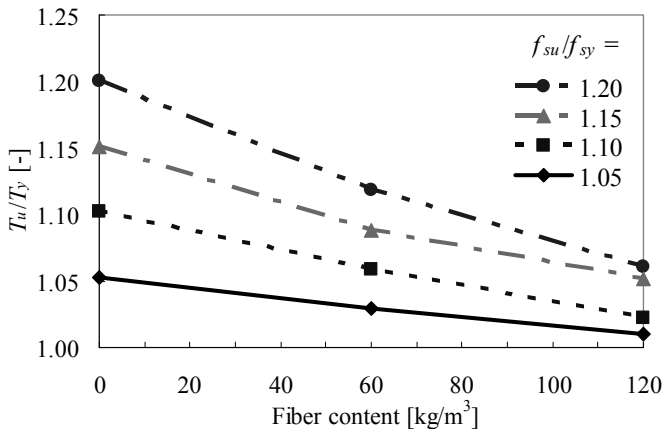

Figure 7: Tensile member hardening ratio for different f_{su}/f_{sy} and fibre contents

6 Rotation capacity tests

6.1 Test set-up

In order to investigate the effect of steel fibres on the rotation capacity of reinforced concrete beams, four beams (height h = 300 mm, width b = 150 mm, total beam length l_0 = 3000 mm, span l = ca. 2850 mm) were loaded at mid-span up to failure (rupture of a steel bar in case of steel failure or pronounced drop in load carrying capacity in case of concrete failure). The beams were reinforced with two ribbed bars with a diameter of 10 mm (ρ = 0.39%). Test variables were fibre content (no fibres and 60 kg/m³ fibres with length l_f = 30 mm and aspect ratio l_f/d_f = 80) and axial compressive force (N = 0 and N = -400 kN). The loading was deformation controlled. Fig. 9 shows the test set-up. Fig. 10 shows the linear

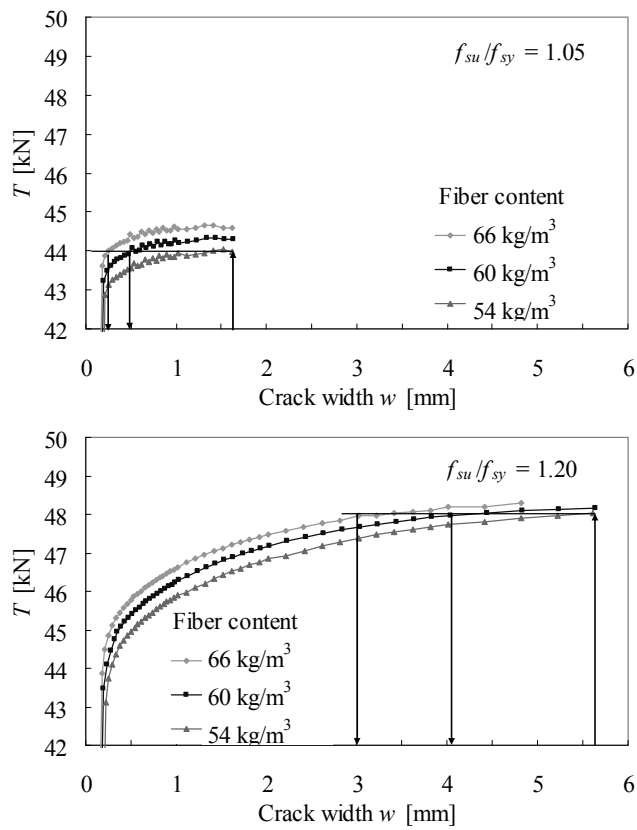

Figure 8: Relation between tensile member force and crack width for steel hardening ratio f_{su}/f_{sy} 1.05 (top) and 1.20 (bottom) and a variation of the fibre content of ± 10%

variable displacement transducers (LVDTs) for measuring the deflections on top of the specimen and the longitudinal displacements at both sides of the specimen at different levels.

*6.2 **Test results***

Fig. 11 and Fig. 12 show the moment in the centre of the beam and the rotation over the entire span, for the tests without (N0) and with (N400) applied axial compressive force. The figures show the stiffer behaviour of the fibre reinforced beams in the ascending branch. The specimens without fibres had a larger rotation capacity than those with fibres. This decrease in deformation capacity is explained by localization of the deformations in one large crack in case of the SCSFRC specimens, contrary to several large cracks in case of

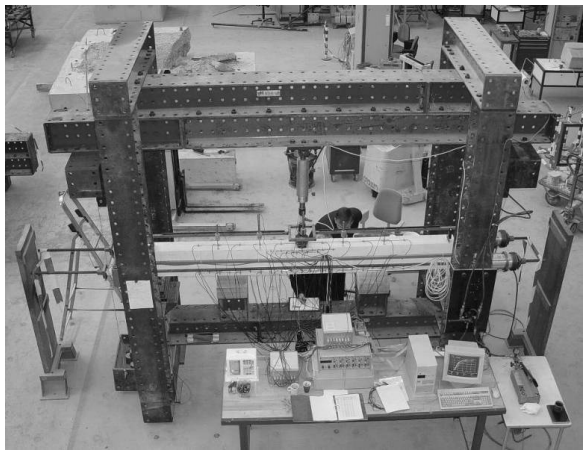

Figure 9: Beam test set-up

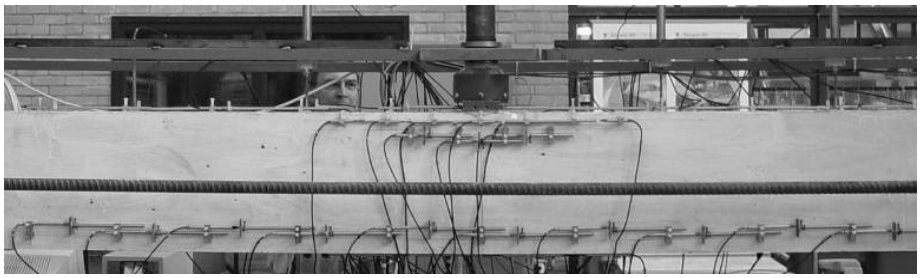

Figure 10: Deflection and strain measurements

the RC specimens. The maximum moment was approximately 10% larger in the fibre reinforced beams than in those without fibres.

Fig. 13 and Fig. 14 show the crack pattern developed in the middle 1200 mm of the beams that were tested without axial compressive force. For better visibility, the cracks were marked with a black line directly next to the actual cracks. The numbers along the cracks indicate the load steps. In Tab. 1 and Tab. 2, the crack widths at the load step before failure are presented. The crack widths for all load steps can be found in Schumacher (2006).

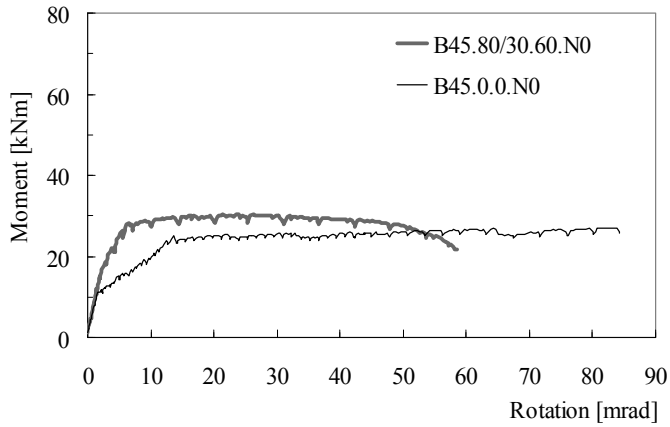

Figure 11: Moment-rotation relation without axial compressive force (N0)

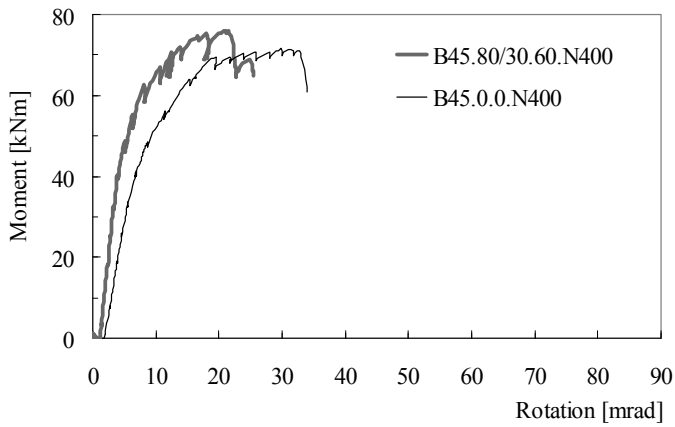

Figure 12: Moment-rotation relation with axial compressive force of -400 kN (N400)

In the SCC specimen B45.0.0.N0, a total number of 18 cracks was observed in the middle 1200 mm of the beam. The average crack distance s_{cr} amounted to 71 mm, see Fig. 13 and Tab. 1. Up to failure it was not clear whether the specimen would fail due to concrete crushing or steel rupture. Finally, the specimen failed due to concrete crushing. The deformations localized in four large cracks (number 6, 7, 9 and 13).

In the SCSFRC specimen B45.80/30.60.N0, a total number of 23 cracks were observed in the middle 1200 mm of the beam. The average crack distance s_{cr} amounted to 55 mm, see Fig. 14 and Tab. 2. The specimen failed due to rupture of a steel bar. The deformations localized in one large crack (number 10). It can be seen that the crack spacing in the SCSFRC was much smaller than that of the SCC.

Fig. 15 and Fig. 16 show the developed crack pattern in the middle 1200 mm of the beams that were tested with axial compressive force. In Tab. 3 and Tab. 4, the crack widths at the final load step before failure are presented. The crack widths for all load steps can be found in Schumacher (2006).

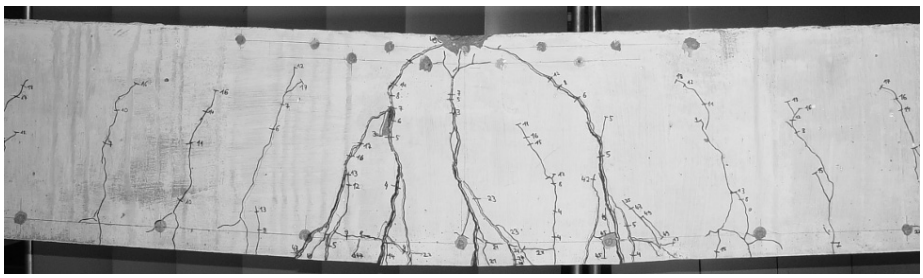

Figure 13: Cracks after testing the beam without normal force without fibres

Table 1: Width w_i [mm], length a_i [mm] and opening angle $\Theta_{cr,i}$ [mrad] of the cracks from left to right just before failure B45.0.0.N0

No.	1	2	3	4	5	**6**	**7**	8	**9**	10	11	12	**13**	14	15	16	17	18
w_i	0.2	0.25	0.2	0.2	0.1	**4**	**5.5**	0.6	**4.5**	1	0.15	1	**4**	1	<	0.35	0.2	0.2
a_i	230	230	210	250	60	**280**	**280**	280	**260**	260	180	280	**280**	280		250	200	210
$\Theta_{cr,i}$	0.9	1.1	1.0	0.8	1.7	**14.3**	**19.6**	2.1	**17.3**	3.9	0.8	3.6	**14.3**	3.6		1.4	1	1.0

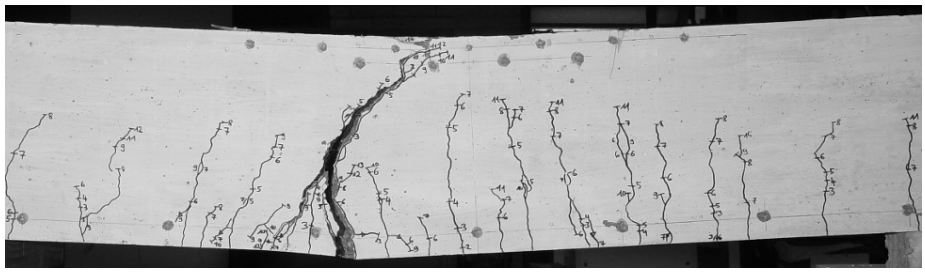

Figure 14: Cracks after testing the beam without normal force with fibres

Table 2: Width w_i [mm], length a_i [mm] and opening angle $\Theta_{cr,i}$ [mrad] of the cracks from left to right just before failure B45.80/30.60.N0

No.	1	2	3	4	5	6	7	8	9	**10**	11	12	13	14	15	16	17	18	19	20	21	22	23
w_i	0.05	0.1	0.05 <		0.05 <		<		<	**14**	0.05 <		0.1	0.05	0.05	0.05	0.05	0.05 <		<	0.05	0.1	0.05
a_i	170	160	180		160					**280**	130		230	100	210	200	200	200			150	160	160
$\Theta_{cr,i}$	0.3	0.6	0.3		0.3					**50**	0.4		0.4	0.5	0.2	0.3	0.3	0.3			0.3	0.6	0.3

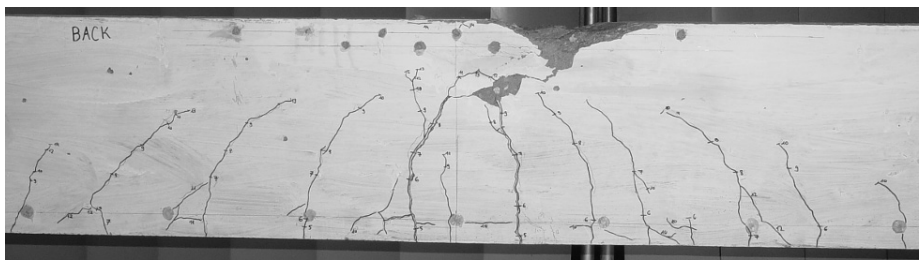

Figure 15: Cracks after testing the beam with normal force without fibres

Table 3: Width w_i [mm], length a_i [mm] and opening angle $\Theta_{cr,i}$ [mrad] of the cracks from left to right just before failure B45.0.0.N400

No	1	2	3	4	5	**6**	7	**8**	9	10	11	12	13	14
w_i	0.05	0.25	0.35	0.35	<	**2**	0.1	**2.3**	0.35	0.3	<	0.35	0.2	<
a_i	130	170	180	220		**220**	120	**220**	200	190		170	150	90
$\Theta_{cr,i}$	0.4	1.5	2.0	1.6		**9.1**	0.8	**10.5**	1.8	1.6		2.1	1. 3	

In the SCC specimen B45.0.0.N400, a total number of 14 cracks were observed in the middle 1200 mm of the beam (1200 mm). The average crack distance s_{cr} amounted to 92 mm, see Fig. 15 and Tab. 3. The specimen failed due to concrete crushing with a large spalling zone. The deformations localized in two large cracks (number 6 and 8).

In the SCSFRC specimen B45.80/30.60.N400, a total number of 32 cracks were observed in the middle 1200 mm of the beam. The average crack distance s_{cr} amounted to 39 mm, see Fig. 16 and Tab. 4. The specimen failed due to concrete crushing showing cracks but no concrete spalling. The deformations localized in one large crack (number 20 in Tab. 4).

*6.3 **Fibre distribution and fibre orientation within the specimens***

For SCSFRC, the direction of casting may influence the fibre distribution and orientation, and therefore the bending behaviour. In order to obtain detailed information on the fibre distribution and fibre orientation in the present tests, some cross-sectional saw cuts were made after testing and pictures were taken of the sawing faces, see Fig. 17.

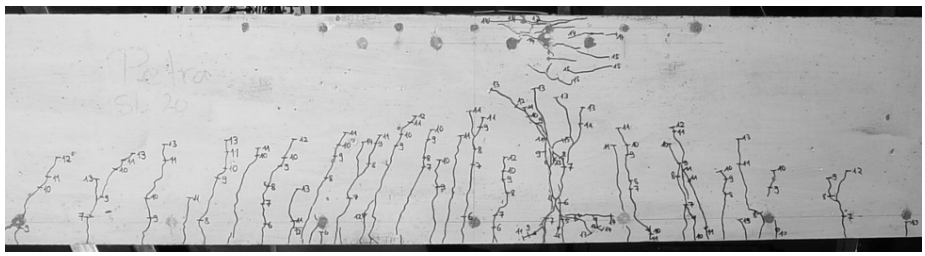

Figure 16: Cracks after testing the beam with normal force with fibres

Table 4: Width w_i [mm], length a_i [mm] and opening angle $\Theta_{cr,i}$ [mrad] of the cracks from left to right just before failure B45.80/30.60.N400

No.	1	2	3	4	5	6	7	8	9	10	11	12	13	14	15	16	17	18	19	**20**	21	22	23	24	25	26	27	28	29	30	31	32
w_i	<	0.1	<	<	<	0.05	<	<	<	<	<	<	<	<	<	0.05	<	<	<	**3.1**	<	<	<	<	<	<	<	<	<	<	<	0.05	<
a_i		120				120										100				**200**	150											100	
$\Theta_{cr,i}$		0.8				0.4										0.5				**15.5**												0.5	

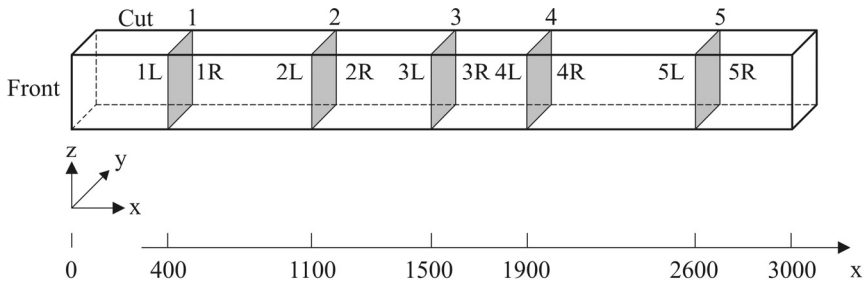

Figure 17: Identification of the saw cuts of the SCSFRC beams

The pictures were taken in a dark room using a camera flash so the fibres reflected the flash and became very well visible. These pictures were analyzed with the optical analysis program Optimas. Areas of a certain colour (fibres) were identified according to predefined threshold values for the colours. The fibres are identified as ellipses and information on their major and minor axis lengths as provided by the software. From the lengths of the axes and the angle with respect to the principal axes of the ellipse, the fibre orientations in the different directions were determined. The number of fibres in the cross-sections was also counted.

The number of fibres assuming a 3D distribution with a fibre orientation factor of 0.5 should be 3.40 per cm². The number of fibres observed in the different cross-sections varied from 2.57 to 3.93 fibres per cm². On average, the observed number of fibres in a picture was slightly lower than the number of fibres expected for a 3D distribution. This can be explained by the fact that the fibres near the edges of the cross-section were not reflected well and therefore not recognized in the optical analysis. The observed number of fibres did not systematically change over the length of the beam.

The observed fibre orientations also did not significantly nor systematically change along the length of the beam. The fibres had a preferred orientation parallel to the *x*-axis as shown in Fig. 17, which can be attributed to the wall effect of the formwork during casting and the flow direction of the concrete. Therefore, the orientation number in the *x*-direction is significantly larger than in the *y*- and *z*-direction. The orientation in the *x*-direction is significant for the tensile behaviour in the cracks of the beams, whereas the orientation in the *y*- and *z*-direction is significant for the tensile forces perpendicular to the compressive

force in the compressive zone of the beams. For further analysis, the orientation number used is 0.68 in the x-direction and 0.43 in the y- and z-direction.

The number of fibres as well as the fibre orientations did not significantly or systematically vary over the beam height. Therefore, the concrete properties were assumed to be constant over the beam height.

7 Rotation modelling

A model for the rotation capacity of plastic hinges has been developed for SCSFRC similar to the models of Bigaj (1999) and Langer (1987) and Li (1997) for RC. The model takes into account bending cracks (perpendicular to the bar axis). It does not take into account the formation of shear cracks (inclined cracks). The possibility of no crack directly under the load but two cracks immediately next to it, as had been investigated by Bigaj (1999), has not been considered in this model. The general procedure for the calculation of the behaviour of a plastic hinge in concrete represents a lower bound approach and can be summarized in the following steps:

Step 1: The material properties and the cross-sectional dimensions are specified.
Step 2: The average crack distance is determined.
Step 3: The steel and concrete strain in the cracked cross-sections of the tensile zone are determined.
Step 4: The concrete strains in the compressive zone of the cracked cross-sections are determined.
Step 5: The average curvature in an element between two subsequent cracks is determined.
Step 6: The rotation is calculated at different load levels.
Step 7: The plastic rotation is calculated.

*7.1 **Step 1: Material and geometry input***

The model used for the calculation of the rotation capacity is based on the assumptions for the compressive behaviour, tensile behaviour and bond as described in the earlier sections. The stress-deformation relation of the steel is simplified by a 4-point polygon. The input values are taken from standard tests, if available.

The stress-deformation relation of the concrete in tension is described by a 4-point polygon relation, with a linear ascending branch (stress-strain relation) and a bilinear descending branch (stress-crack width relation, see Fig. 1). Due to the anisotropy of the SCSFRC, the contribution of a fibre in different directions varies with the angle between the fibre and the crack. In the present model, the properties of concrete in tension are explicitly defined in two distinct directions: parallel and transverse to the beam axis. This provides the possibility to take into account the fibre orientation within the specimen. In this way a distinction is made between the influences of the fibres on the confinement capacity on the one hand and on the load transfer across the cracks on the other hand. For assessing the confinement of the ribbed bars, the average concrete properties around a bar are relevant. For the estimation of the contribution to the tensile force transfer of the concrete and the steel along the beam, the statistical variation of the concrete tensile properties, which was shown in section 6.3, might be taken into account by varying the input parameters. The stress-strain relation in the cracks is obtained by dividing the crack width of the stress-crack opening relation by the average crack distance.
The stress-deformation relation of concrete in compression is specified as a 5-point polygon. The model is developed for rectangular cross-sections. The geometry of the specimen is specified by its width, depth, distance from bottom to the centre of gravity of the reinforcing bars, total length of the specimen, span, steel bar reinforcement diameter and number of steel bars.

7.2 Step 2: Average crack distance s_{cr}

In the model for the rotation capacity, the transmission length L_t and the average crack distance s_{cr} are calculated with the bond model presented in section 4. In the model for the rotation capacity it is assumed that the first crack forms in the cross-section at the load axis and that the subsequent cracks form symmetrically to both sides at the average crack distance s_{cr}. The number of cracks is therefore uneven.

7.3 Step 3: Steel and concrete strains in the tensile zone

For the calculation of the steel and concrete strain distribution in a tensile element between two subsequent cracks, the differential equation of bond is solved through finite difference calculus, see Chapter 4. For the calculation of bending members, the boundary conditions are:

Different tension chord forces at both ends of the element between two subsequent cracks correlated to the moment gradient. The tensile chord force T_1 at the position along the beam with a larger moment is larger than the tensile chord force T_2 at the position with the smaller moment. The difference between the two forces reflects a shear force S, which is assumed to act uniformly distributed over the length of the element, see Fig. 18. The concrete stress at the beginning and at the end of the element between two subsequent cracks are a function of the slip, see also section 4.3.

The calculation is performed in the following substeps: For a predefined slip, the steel stress in the first crack is varied in a number of iterations until equilibrium of forces is found and the tension chord forces at both ends of the element between two subsequent cracks satisfy the relation depending on the moment gradient, taking into account that the calculated slip in the second crack corresponds to the concrete stress at that crack. The steel strain is then calculated from the steel stress and the concrete strain at the height of the reinforcing bars is calculated by dividing the crack width w, which is twice the slip δ, by the crack distance s_{cr}.

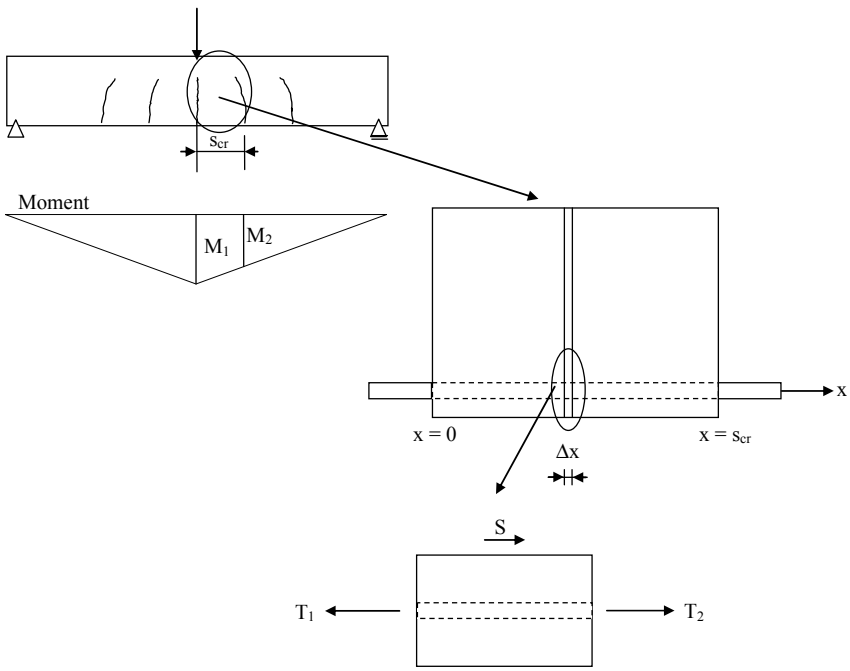

Figure 18: Illustration of the shear force in an element between two subsequent cracks due to a moment gradient

7.4 Step 4: Concrete strains in the compression zone in the cracked cross-section

For each set of the previously calculated steel strains and concrete strains at the height of the reinforcing bar, the concrete strains in the compressive zone of the cracked cross-sections are calculated following an iterative procedure in a cross-sectional analysis with the help of a layer model. The cross-section is divided into 100 layers from top to bottom. The strain distribution over the beam height and the corresponding moment and curvature are calculated in the following steps:

- The concrete strain in the compressive zone is varied until equilibrium of inner and outer forces (normal force and moment) is found.
- The position of the neutral axis is determined by a line connecting the concrete strain in the most stressed fibre with the previously determined steel strain.
- The strain distribution in the concrete in the compressive zone is assumed linear from the most compressed fibre to the neutral axis.
- The concrete strain in the tensile zone is assumed to be linear crossing zero at the neutral axis and the previously calculated concrete strain at the level of the reinforcing bar.
- For each layer the normal force is calculated from the strains and the material input.
- The curvature is calculated from the concrete strain in the compression zone and the steel strain in the tensile zone.

It is noted that for SFRC, the steel and the fibre reinforced concrete contribute to the force transfer in the tensile zone, whereas the concrete contribution in concrete without fibres is negligible, see section 3.3. The stress development was illustrated in Fig. 4. This strain distribution is illustrated in Fig. 19.

For each set of steel and concrete strains at the height of the reinforcing bar, the moment and the curvature are calculated for the given dimensions and material properties, rendering the ascending and descending branch of the moment-curvature relation.

The failure criteria are related to the strain at the top (concrete crushing) and the strain at the level of the bar reinforcement (steel rupture). Steel failure is assumed to occur when the steel strain reaches the ultimate steel strain. Concrete failure is assumed to occur when the strain in the most compressed layer reaches the maximum concrete compressive strain. Whichever happens first, determines the failure mechanism.

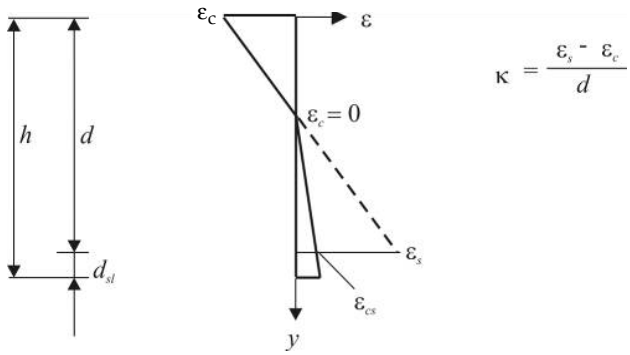

Figure 19: Strain distribution of concrete and steel in the crack

It is noted that the calculation of the strain at which the stress becomes zero in the post-peak range depends on the damage zone length L_d and that the calculation is therefore an iterative procedure. In every step of calculating the moment-curvature relation, the damage zone length L_d is first assumed to be zero and the stress-strain relation is calculated. With this relation, the cross-sectional analysis is done, which yields the damage zone depth d_l and the new damage zone length L_d. The previous damage zone length is compared with the new one. In case of disagreement, the new one is used to calculate the stress-strain relation and perform the cross-sectional analysis. This procedure is followed until sufficient agreement of the previous and the new damage zone length is reached.

*7.5 **Step 5: Average curvature in an element between two subsequent cracks***

The average curvature in an element between two subsequent cracks is determined by the difference between average steel strain in the element and the concrete compressive strain in the crack divided by the effective height of the cross-section.

It is noted that this procedure can lead to an overestimation of the curvature, because in reality the concrete strains in the compressive zone between the cracks are lower. This overestimation is considered acceptable because in case of steel failure, the main contribution to the curvature is found in the large steel strains (at failure approximately 100‰ compared to approximately 4‰ for concrete). In case of concrete failure, the damage zone was found to be larger than the crack spacing and therefore extends into the element. Thus the concrete strain is constant for the length of the plastic hinge and the assumption is correct.

7.6 Step 6: Total rotation of the beam

The total rotation of the beam is the integration of the curvature along the beam according to equation (7):

$$\Theta = \int_0^l \kappa \, dx \tag{7}$$

This is obtained by multiplying the average curvature of each element between two subsequent cracks from step 5 with the average crack distance s_{cr}. These rotations are added in order to obtain the rotation of the beam.

7.7 Step 7: Calculation of the rotation capacity

The rotation capacity was defined in chapter 2 as the difference between the total rotation at maximum load minus the rotation at the onset of steel yielding according to equation (8):

$$\Theta_{pl} = \Theta_{tot} - \Theta_{el} \tag{8}$$

For comparison, the total rotation at failure minus the rotation at the onset of steel yielding is also calculated and presented.

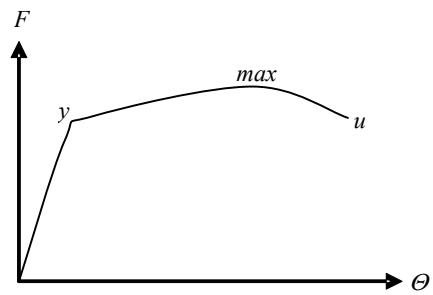

Figure 20: Definition of the significant load steps

8 Comparison of model and experiments

8.1 Rotations at different load steps

The model has been validated for SCC and SCSFRC members in bending. For this, three load steps have been considered: the onset of steel yielding (y), the maximum load (max) and the ultimate load (u), see Fig. 20.

Tab. 5 and Fig. 21 show the results of the model validation for the measured and calculated rotations at the onset of yielding, at maximum load and at ultimate load. Due to a plateau at maximum loading in the fibre reinforced specimens, the rotation of the maximum load and the rotation capacity are given as a range in the tables as well as in the figures. The calculated rotations agree well with the measured ones.

8.2 Rotation capacity and rotation at ultimate load minus rotation at the onset of steel yielding

The rotation capacity ($\Theta_{max}-\Theta_y$) and the difference between the rotation at ultimate load and the rotation at the onset of steel yielding ($\Theta_u-\Theta_y$) were derived from the calculated rotations. The values are given in Tab. 6 and are illustrated in Fig. 22. The influence of steel fibres on the difference of the rotations at ultimate load minus the rotations at the onset of steel yielding has also been investigated because in structures which allow for redistribution of forces at decreasing load bearing capacity in the plastic hinges, the descending branch of the moment-curvature relation is also of interest. The rotation capacity of the beams ($\Theta_{max}-\Theta_y$) observed in the experiments is slightly underestimated by the calculation model. The rotations at ultimate load minus the rotations at the onset of steel yielding obtained in the calculations are also underestimated.

8.3 Effect of fibres in the tests without axial compressive force

For the investigated parameters, the experiments as well as the parameter studies showed that the overall rotation capacity in the tests without normal force was significantly decreased when fibres were added. This phenomenon had already been observed for tensile members by other researchers, e.g. Pfyl & Marti (2001), Eligehausen et al. (2003), Fehling & Leutbecher (2005). The rotation at ultimate load minus the rotation at the onset of steel yielding in the tests without normal force was decreased when fibres were added in both the experiment as well as the simulations, compare specimen B45.0.0.N0 to B45.80/30.60.N0.

Table 5: Measured and calculated rotations at onset of yielding (y), maximum (max) and ultimate load (u)

Test	$\Theta_{measured}$ at F_y [mrad]	$\Theta_{calculated}$ at F_y [mrad]	$\Theta_{measured}$ at F_{max} [mrad]	$\Theta_{calculated}$ at F_{max} [mrad]	$\Theta_{measured}$ at F_u [mrad]	$\Theta_{calculated}$ at F_u [mrad]
B45.0.0.N0	14	14	83	68	83	68
B45.80/30.60.N0	8	13	15-37	22	59	54
B45.0.0.N400	19	19	33	27	33	27
B45.80/30.60.N400	10	16	20-22	26	27	26

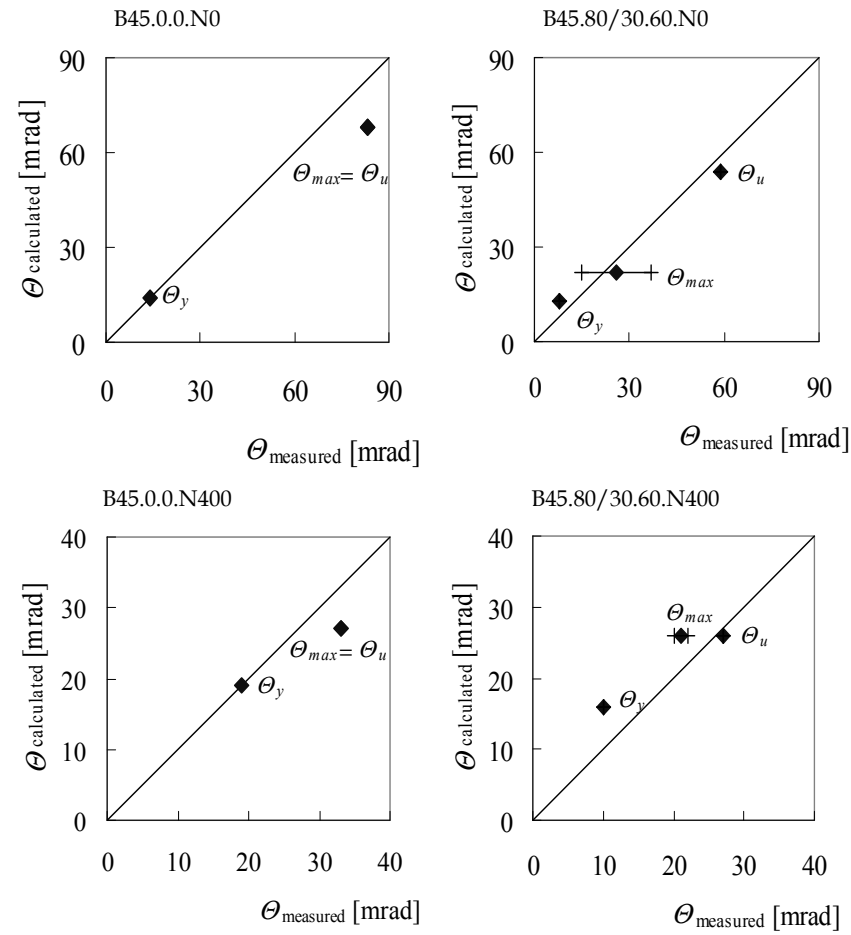

Figure 21: Comparison of calculated and measured rotations at different load steps

Table 6: Rotation capacity and difference between rotation at ultimate load and rotation at the onset of steel yielding from the tests and the calculations

Test	$\Theta_{max}-\Theta_y$ measured [mrad]	$\Theta_{max}-\Theta_y$ calculated [mrad]	$\Theta_u-\Theta_y$ measured [mrad]	$\Theta_u-\Theta_y$ calculated [mrad]
B45.0.0.N0	68	55	68	55
B45.80/30.60.N0	8-29	9.4	51	41
B45.0.0.N400	14	8.6	14	8.6
B45.80/30.60.N400	10-12	9.1	17	9.1

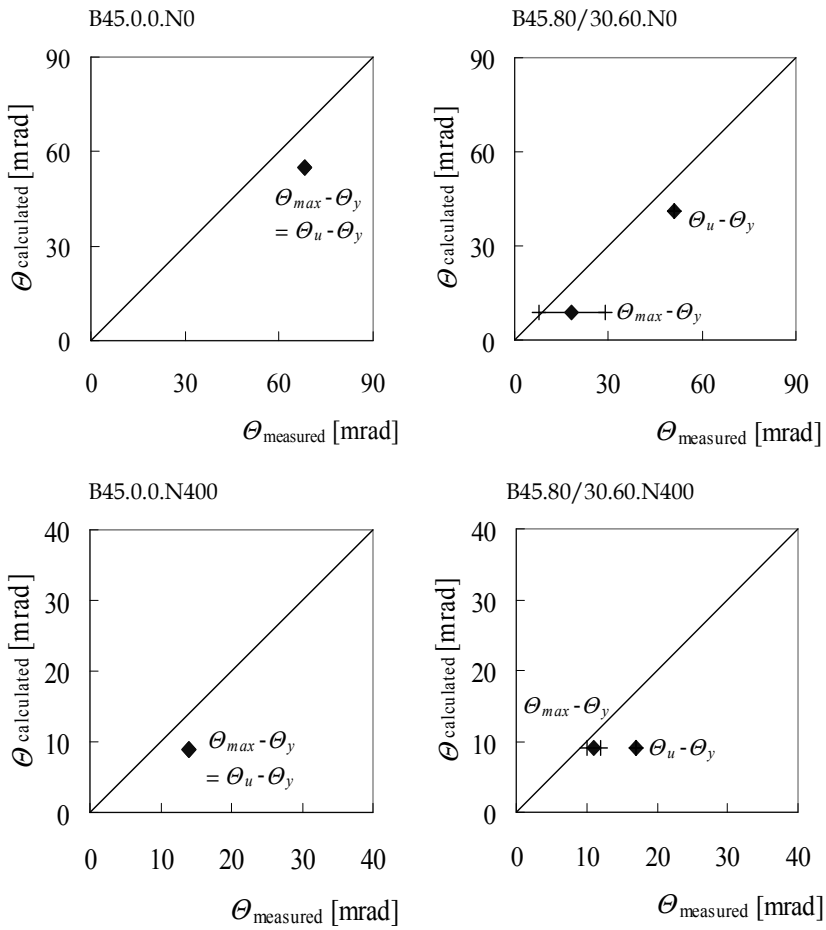

Figure 22: Comparison of calculated and measured rotation capacity and difference between rotation at ultimate load and rotation at the onset of steel yielding

8.4 Effect of fibres in the tests with axial compressive force

For concrete failure, the experimentally observed rotation capacity did not significantly decrease due to the fibre addition, compare specimen B45.0.0.N400 to B45.80/30.60.N400. The experimental and calculation results seem contradictory. However, the difference is not significant. It should be understood that in compressive failure, the two phenomena of increased deformation capacity in compression and localization of the deformations in one large crack counteract. The rotation at ultimate load minus the rotation at the onset of steel yielding was slightly increased in the experiments due to the fibre addition. This increase is attributed to the increase in concrete ductility in compression due to fibre addition.

9 Conclusions

The following conclusions can be drawn from the experiments and parameter studies:

1. The increase of the ductility of concrete in compression due to fibre addition depends, among other factors, on the amount, geometry, orientation and strength of the steel fibres and the bond between fibres and concrete. With the proposed extension of the Compressive Damage Zone Model of Markeset (1993) for different amounts and aspect ratios of hooked-end steel wire fibres, the influence of these factors can be well captured.
2. The addition of steel fibres does not significantly affect the bond stress-slip relation of reinforcing bars in case of pull-out bond failure.
3. The addition of steel fibres leads to stiffer member behaviour and smaller crack widths in the SLS.
4. The addition of steel fibres leads to a reduction in crack spacing and to an increased load bearing capacity of tensile members and bending beams in the ULS.
5. The addition of steel fibres did not prevent longitudinal crack formation in the compressive zone in case of compressive failure, but it prevented concrete spalling.
6. Depending on the combination of steel fibres (amount, geometry, orientation, bond properties) and reinforcing bars (amount, hardening properties), localization of the deformations in one crack can occur. In case of localization of the deformations in one crack, the total deformations at failure are smaller than for the specimens without fibres where localization occurs in several cracks.
7. The model for the calculation of the rotation capacity was suitable to simulate the deformation behaviour of SCSFRC members with ordinary reinforcement.

Hence it has been demonstrated that the deformation capacity can be predicted with tension, compression and bond models that are based on a physically correct basis and validated for the range of the material.

Acknowledgement

The financial support of Delft Cluster (project 01.06.03) is gratefully acknowledged as well as the donation of the steel fibres by the Belgian company Bekaert and the support of the technical staff in the Stevin laboratory.

References

Bigaj, A.J. (1999). *Structural Dependence of Rotation Capacity of Plastic Hinges in RC Beams and Slabs*, PhD thesis, Delft University of Technology.

CEB (1998). *Ductility of reinforced concrete structures, Synthesis report and individual contributions*, Bulletin 242, Lausanne, Switzerland.

Eligehausen, R., Mayer, U., Lettow, S. (2003). *Mitwirkung des Betons zwischen den Rissen in Stahlbetonbauteilen*, Abschlussbericht zum DFG-Forschungsvorhaben EL 72/8-1+2, Universität Stuttgart, Germany.

Eurocode 2 (1992). *Planung von Stahlbeton- und Spannbetontragwerken*. ENV 1992-1-1: 1991.

Fehling, E., Leutbecher, T. (2005). *Structural behaviour of UHPC under tension, using steel fibres and bar reinforcement*, unpublished presentation.

Grünewald, S. (2004). *Performance-based design of self-compacting fibre reinforced concrete*, PhD Thesis, Delft University of Technology, The Netherlands.

Gysel, A. van (2000). *Studie van het uittrekgedrag van staalvezels ingebed in een cementgebonden matrix met toepassing op staalvezelbeton onderworpen aan buiging*, Universiteit Gent, Doctoral Thesis, Academiejaar 1999-2000.

Hartwich, K. (1986). *Zum Riss- und Verformungsverhalten von stahlfaserverstärkten Stahlbetonstäben unter Längszug*, Dissertation, TU Braunschweig, Institut für Baustoffe, Massivbau und Brandschutz, Heft 72, Germany.

Kützing, L. (2000). *Tragfähigkeitsermittlung stahlfaserverstärkter Betone*, B.G.Teubner Stuttgart Leipzig Wiesbaden.

Langer, P., (1987). Verdrehfähigkeit *plastizierter Tragwerksbereiche im Stahlbetonbau*, Dissertation, Universität Stuttgart, Institut für Werkstoffe im Bauwesen, 1987/1, Germany.

Li, L., (1997). *Rotationsfähigkeit von plastischen Gelenken im Stahl- und Spannbetonbau*, Deutscher Ausschuß für Stahlbeton, Heft 484, Beuth Verlag GmbH, Germany, pp. 45-126.

Markeset, G. (1993). *Failure of concrete under compressive strain gradients*, Dr.ing. Thesis 1993: 110, The Norwegian Institute of Technology, Trondheim.

Marković, I., Grünewald, S., Walraven, J.C., Mier, J.G.M. van (2002). Characterization of Bond Between Steel Fibres and Concrete – Conventional Fibre Reinforced Versus Self-Compacting Fibre Reinforced Concrete, in: *Bond in Concrete – from research to standards*, Balázs, G. et al. (ed.), pp. 520-528.

Niemann, P. (2002). *Gebrauchsverhalten von Bodenplatten aus Beton unter Einwirkung infolge Last und Zwang*, Dissertation, TU Braunschweig, Germany.

Pfyl, Th., Marti, P. (2001). *Versuche an stahlfaserverstärkten Stahlbetonelementen*, Institut für Baustatik und Konstruktion, ETH Zürich, Switzerland, IBK Bericht Nr. 268, Birkhäuser Verlag, Basel, 137 pp.

Pfyl, Th. (2003). *Tragverhalten von Stahlfaserbeton*, Dissertation ETH Nr. 15005, Switzerland.

Schumacher, P. (2006). *Rotation Capacity of Self-Compacting Steel Fibre Reinforced Concrete*, PhD Thesis, Delft University of Technology, The Netherlands.

Tepfers, R. (1979). Cracking of concrete cover along anchored deformed reinforcing bars, *Magazine of Concrete Research*, Vol. 31, No. 106, pp. 3-12.

Uijl, J.A. den, Bigaj, A.J. (1996). A bond model for ribbed bars based on concrete confinement, *Heron*, Vol. 41, No. 3, pp. 201-226.

Symbols

Roman capital letters

$A_{c,eff}$	Effective concrete tension area	[mm²]
A_s	Steel cross-section	[mm²]
E_c	E-modulus of concrete	[N/mm²]
E_s	E-modulus of steel	[N/mm²]
F	Force	[kN]
F_{max}	Maximum force	[kN]
F_u	Force at failure	[kN]
F_y	Force at the beginning of steel yielding	[kN]
L_d	Damage zone length	[mm]

L_t	Transmission length	[mm]
L_{tf}	Transmission length of concrete with fibres	[mm]
N	Normal force	[kN]
S	Shear force in element between two subsequent cracks	[N]
T	Tensile member force or tensile chord force	[N]
T_1	Tensile chord force at crack 1	[N]
T_2	Tensile chord force at crack 2	[N]
T_y	Tensile member force at the beginning of steel yielding	[N]
T_u	Tensile member force at failure	[N]
U_s	Circumference of the steel bar	[mm]
V_f	Fibre content	[m^3/m^3]

Roman Lower Case Letters

a	Crack length	[mm]
b	Width of a cross-section	[mm]
c	Clear concrete cover on the bar	[mm]
d	Effective height of a cross-section	[mm]
d_f	Fibre diameter	[mm]
d_l	Depth of the compressive damage zone	[mm]
d_s	Steel bar diameter	[mm]
d_{s1}	Height h minus effective height d	[mm]
f_c	Concrete cylinder or prism compressive strength	[N/mm^2]
f_{ct}	Concrete tensile strength	[N/mm^2]
f_{su}	Ultimate tensile strength of steel	[N/mm^2]
f_{sy}	Yield strength of steel	[N/mm^2]
h	Height of a cross-section	[mm]
i	Ordinal integer number	[-]
k	Proportionality factor	[-]
l	Span	[mm]
l_f	Fibre length	[mm]
l_0	Total beam length	[mm]
n_E	Ratio of E-moduli of steel and concrete	[-]
s_{cr}	Crack spacing	[mm]
w	Crack width	[mm]

w_0	Critical crack width	[mm]
x, y, z	Cartesian coordinate system	[-]

Greek Capital Letters

Δx	Element length	[mm]
Θ	Rotation	[mrad]
Θ_{el}	Elastic rotation	[mrad]
$\Theta_{cr,i}$	Crack opening angle of a crack	[mrad]
Θ_{max}	Rotation at maximum load	[mrad]
Θ_{pl}	Plastic rotation	[mrad]
Θ_{tot}	Total rotation	[mrad]
Θ_u	Rotation at ultimate load	[mrad]
Θ_y	Rotation at the onset of steel yielding	[mrad]

Greek Lower Case Letters

α_{FCM}	Constant (FCM)	[-]
β_{FCM}	Constant (FCM)	[-]
δ_x	Slip	[mm]
ε	Strain	[-]
ε_c	Strain in the compressive zone	[-]
ε_s	Steel strain	[-]
ε_{su}	Ultimate steel strain	[-]
ε_t	Strain in the tensile zone	[-]
κ	Curvature	[1/km]
ρ	Geometrical reinforcement ratio	[%]
σ	Stress	[N/mm²]
σ_{ct}	Concrete tensile stress	[N/mm²]
σ_{cx}	Concrete stress	[N/mm²]
σ_{sx}	Steel stress	[N/mm²]
τ_b	Bond stress	[N/mm²]
τ_x	Bond stress	[N/mm²]
τ_{b1}	Threshold value pull-out or splitting bond failure	[N/mm²]
ω_s	Mechanical reinforcement ratio	[-]

Abbreviations

CDZ	Compressive Damage Zone
FCM	Fictitious Crack Model
LVDT	Linear Variable Displacement Transducer
RC	Reinforced concrete
SCC	Self compacting concrete
SCSFRC	Self compacting steel fibre reinforced concrete
SFRC	Steel fibre reinforced concrete
SLS	Serviceability Limit State
ULS	Ultimate Limit State